

Process Variability and Electrostatic Analysis of Molecular QCA

Original

Process Variability and Electrostatic Analysis of Molecular QCA / Graziano, Mariagrazia; Pulimeno, Azzurra; RUO ROCH, Massimo; Wang, Ruiyu; Piccinini, Gianluca. - In: ACM JOURNAL ON EMERGING TECHNOLOGIES IN COMPUTING SYSTEMS. - ISSN 1550-4832. - ELETTRONICO. - 12:2(2015), pp. 18:1-18:23. [10.1145/2738041]

Availability:

This version is available at: 11583/2625634 since: 2015-12-15T04:04:13Z

Publisher:

ACM

Published

DOI:10.1145/2738041

Terms of use:

This article is made available under terms and conditions as specified in the corresponding bibliographic description in the repository

Publisher copyright

ACM postprint/Author's Accepted Manuscript, con Copyr. autore

© Graziano, Mariagrazia; Pulimeno, Azzurra; RUO ROCH, Massimo; Wang, Ruiyu; Piccinini, Gianluca 2015. This is the author's version of the work. It is posted here for your personal use. Not for redistribution. The definitive Version of Record was published in ACM JOURNAL ON EMERGING TECHNOLOGIES IN COMPUTING SYSTEMS, <http://dx.doi.org/10.1145/2738041>.

(Article begins on next page)

Process Variability and Electrostatic Analysis of Molecular QCA

M. Graziano, London Centre for Nanotechnology

A. Pulimeno, R. Wang, X. Wei, M. Ruoch, G. Piccinini, Politecnico di Torino

Molecular Quantum-dot Cellular Automata (mQCA) is an emerging paradigm for nanoscale computation. Its revolutionary features are the expected operating frequencies (THz), the high device densities, the non-cryogenic working temperature, and, above all, the limited power densities.

The main drawback of this technology is a consequence of one of its very main advantages, i.e. the extremely small size of a single molecule. Device prototyping and the fabrication of a simple circuit are limited by the lack of control in the technological process [Pulimeno et al. 2013a]. Moreover, high defectivity might strongly impact the correct behavior of mQCA devices. Another challenging point is the lack of a solid method for analyzing and simulating mQCA behavior and performance, either in ideal or defective conditions.

Our contribution in this paper is threefold. i) We identify a methodology based on both ab-initio simulations and post-processing of data for analyzing a mQCA system adopting an electronic point of view (we baptized this method as “MoSQuiTo”). ii) We assess the performance of a mQCA device (in this case a bis-ferrocene molecule) working in non ideal conditions. We use as a reference the information on the fabrication critical issues and on the possible defects that we are obtaining while conducting our own ongoing experiments on mQCA. iii) We determine and assess the electrostatic energy stored in a bis-ferrocene molecule both in an oxidized and in a reduced form.

Results presented here consist of quantitative information for a mQCA device working in manifold driving conditions and subjected to defects. These information are given in terms of a) output voltage b) Safe-Operating-Area (SOA), c) electrostatic energy, d) relation between SOA and energy, i.e. possible energy reduction subject to reliability and functionality constraints. The whole analysis is a first fundamental step toward the study of a complex mQCA circuit. It gives important suggestions on the possible improvements of the technological processes. Moreover, it starts an interesting assessment on the energy of a mQCA, one of the most promising feature of this technology.

1. INTRODUCTION

The most important reason why Quantum-dot Cellular Automata elements [Lent et al. 1993] could successfully substitute CMOS devices relies on the information propagation principle. Information transfer among QCA devices is determined only by local field interaction and does not involve charge transport. As a consequence, the power dissipated is dramatically reduced. Notwithstanding the amazing device density allowed by the extremely reduced feature sizes, the power dissipation, and especially the power density, is much less than in CMOS technologies [Pulimeno et al. 2012] and in other emerging technologies based on electron transport [Graziano et al. 2013][Zahir et al. 2014]. This point represents the most promising reason to explore mQCA potentials.

In recent years the QCA principle has been studied, and in some cases experimentally demonstrated, considering a few different technologies, materials and approaches [Lent et al. 1993][Imre et al. 2003][Graziano et al. 2011][Vacca et al. 2012][Awais et al. 2013][Vacca et al. 2014][Awais et al. 2012] (see the next section for a state of the art description). In this work we focus on molecular QCA, which promises nanometer-scale devices, ultra-high device densities, room-temperature operation and, in particular, very low energy dissipation [Blair et al. 2009]. In particular, we study a real molecule, a bis-ferrocene molecule (Figure 1(A)), specifically ad-hoc synthesized for this purpose [Arima et al. 2012] that we adopted for our own experiments. The technological process, though, both in general and specifically for this molecule, is currently lacking

Author's addresses: VLSI Laboratory, Electronics and Telecommunications Department, Politecnico di Torino, corso Duca degli Abruzzi 24, Torino (TO), Italy. Mariagrazia Graziano is also with London Centre for Nanotechnology, Physics and Astronomy Department, UCL, London.

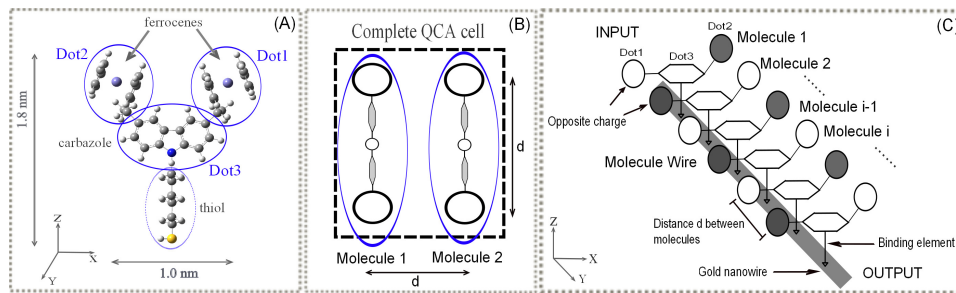


Fig. 1. (A) Bis-ferrocene molecule structure: two ferrocenes are linked together by means of a carbazole central group. These ferrocenes represent the two active dots responsible for the logic state encoding, while the carbazole acts as the central third dot. An alkyl-chain provides the binding of the bis-ferrocene to the ending thiol (-SH) group. This end-group is responsible for the binding to the gold substrate, especially for the Self-Assembled-Monolayer formation. (B) A complete QCA square cell implemented by aligning two bis-ferrocene molecules (*molecule1* and *molecule2*) together with an inter-molecule distance d that equals to the distance between two active dots. (C) Molecular QCA wire structure: bis-ferrocene molecules aligned together with the identical distance d over a gold nanowire through the binding elements.

proper control. This fact explains the extremely reduced set of prototypes and experiments on this QCA type ([Pulimeno et al. 2013a][Li et al. 2003][Qi et al. 2003][J.Jiao et al. 2003]). Hence, it is fundamental to *provide a complete fault tolerance assessment* of QCA device behavior in presence of technological defects. Moreover, a sound *understanding of the electrostatic potential energy stored* in the QCA devices is essential, being the power dissipation issue the most important in any forthcoming technology to be studied in the future. In addition, important *relations between the available energy ranges and the correct operation either in absence or in presence of defects* should be highlighted. This is essential in order to offer the technologist crucial feedbacks on the directions to be followed when refining the process of molecular QCA device implementation.

Regarding the methodological approach the literature shows a few attempts to simulate QCA devices ([Walus][M.Momenzadeh and Lombardi 2005][Tahoori et al. 2004]), sometimes based on models specifically developed for the purpose ([Yang et al. 2012][Schulhof et al. 2007]). However, no systematic approach to analyze mQCA from an electronic point of view has ever been proposed, specifically in the scenario of molecular QCA. We believe that it is essential to put the attention as much as possible close to the physical level and the experimental procedures in order to understand the device behavior as much precisely as possible. Prosecuting the method we started and described in previous papers ([Pulimeno et al. 2013a]), we perform in the present work ab-initio simulations as a first step. Then we proceed with further data elaborations, maintaining the point of view of the electronic engineer, i.e. focusing on the electronic behavior more than on the chemical behavior of the mQCA system.

Inspired by the abovementioned motivations, in this study we refer to an experiment we are preparing for demonstrating the molecular QCA wire (Figure 1(C)). Summarizing our work, the main **contributions and advancement** with respect to the state of the art are as follows:

- a) we defined a proper methodology ("MoSQuiTo") to analyze the molecule behavior based on ab-initio simulations and successive data post-processing to understand the device-level behavior of the molecule and of a molecular wire;
- b) we analyzed the performance of the bis-ferrocene molecule as QCA device from an electronic point of view;

- c) we identified the possible defects and causes of faults considering a real experiment on molecular QCA device based on specific designed molecule;
- d) we defined the Safe-Operating-Area (SOA) to evaluate and assess the capability of the molecule to hold information and to propagate it to a receiver molecule considering real fabrication defects;
- e) we computed the electrostatic energy of molecules when they are not in the equilibrium condition;
- f) we investigated whether a reduced electrostatic potential energy would be involved if a reduction of SOA for molecular QCA wire is allowed.

Results in these directions provide a significant feedback to the technologist to trim the technological process and experimental steps as function of realistic performance. These information contribute to the QCA state of the art with an unprecedented point of view. It is also worth mentioning that the method is general and can be applied to analyze other molecules and experimental setup related to molecular QCA.

This paper is organized as follows: in section 2 we give a background on QCA and on the molecule we are concentrating on. In the meanwhile, we describe the type of defects under consideration of our ongoing experimental procedures. In section 3 we describe the methodology tool “MosQuiTo” and, in particular, the energy analysis. In section 4 we provide the relevant results and comments in order to demonstrate the molecular QCA device performance, and at the last 5 we give our conclusions.

2. BACKGROUND

QCA paradigm. The QCA theory was introduced as a new concept for digital computing [Lent et al. 1993]. According to this theory a new device could be implemented by a cell with 6 dots containing two free charges (Figure 1B). Depending on the positions of the free charges, three different states would be possibly encoded. When the two free charges localize along one of the two diagonals, the logic state “0” and “1” are encoded. The configuration with the two charges forced in the central dots represents a “*NULL*” state, which is not a real logic state, but it is necessary for realizing the adiabatic switching (Figure 2(A)). The Coulomb interaction among electrons provides the digital communication between nearby QCA cells. The local field interaction determines the information transfer without charge transportation. Consequently, the associated power consumption, and in particular the power density, is expected to be dramatically reduced. This remains true notwithstanding the amazing device density that could be expected. This density is remarkably bigger than the one nowadays possible with standard technologies due to the extremely small molecules sizes. Simple QCA logic gate could be implemented by placing QCA cells near each other in a specific layout. The basic logic gates made of QCA cells are shown in Figure 2(B) and Figure 2(C). Using these gates as building blocks many complex digital systems could be designed [Vacca et al. 2011].

Molecular QCA. Regarding the physical implementation, many solutions have been proposed [Imre et al. 2003][Graziano et al. 2011][Qi et al. 2003][Chiolerio et al. 2012]. The smallest and most performing QCA cell could be implemented with a molecular system [Li et al. 2003]. Since many molecules have nanometer size, the device density of a chip could notably increase leading to digital systems with potential high complexity. In addition, theoretical frequencies up to THz are estimated, still assuming a non cryogenic operating temperature.

Recently, the authors in [Arima et al. 2012] synthesized a new molecule (bis-ferrocene molecule) ad-hoc for QCA purpose: the structure of the molecule is reported in Figure 1(A). The bis-ferrocene molecule is constituted by two ferrocene units, where each ferrocene is linked to the next by a carbazole central group. The carbazole group

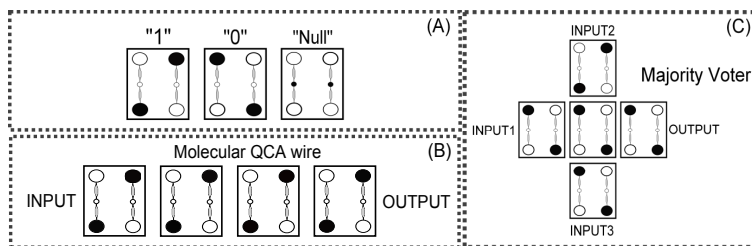


Fig. 2. QCA basic cells and basic logic blocks. (A) Six dots QCA cell: two free charges (filled with black circles) are localized along one of the two diagonal, encoding the “0” or “1” logic state; when the charges are forced by an external signal into the central dots of the cell, the “NULL” state is encoded. (B) A QCA wire: each cell along the line arranges its state according to its neighboring previous cell; when an external input forces a logic state on the first left cell (as INPUT), then the binary information propagates along the whole until reaching to the very right cell (as OUTPUT) in a domino-like style. (C) A majority voter: the output logic state depends on the state of the majority of the three input cells.

shows an alkyl-chain to which an ending sulfur atom, actually a thiol (-SH), is attached. This end-group is responsible for the interaction with the gold substrate for the self assembled monolayer (SAM) formation, if fabricated using gold (see later a further explanation). Particularly, the two ferrocenes represent the dots responsible for boolean encoding [Pulimeno et al. 2011]. They are called the two active dots (hereinafter named *Dot1* and *Dot2*). The carbazole acts as a central dot (hereinafter named *Dot3*) for the “NULL” state encoding. Regarding the QCA cell and its functionality, since the bis-ferrocene molecule has only three dots, it could be considered as half QCA cell. A complete QCA cell could be implemented placing two molecules near each other in such a way to obtain a squared with the four boolean dots, as depicted in Figure 1(B). The molecule is always neutral. A better performance could be obtained by its oxidized (a positive net charge inside the molecule) or reduced form (a negative net charge inside the molecule) of the same molecule.

Fabrication defects. As mentioned in [Pulimeno et al. 2013a], in order to experimentally demonstrate the QCA functionality, we are preparing a bis-ferrocene molecular wire like the one in Figure 1(C). It is based on a gold nanowire on top of which the molecules can be binded through the thiol element [Fenwick et al. 2009][Rattalino et al. 2012][Strobel et al. 2009][Motto et al. 2014][Casu et al. 2004]. The exact experiment description can be found in [Pulimeno et al. 2013a].

During the gold substrate preparation and the molecule deposition (SAM), some defects may occur and they are schematically sketched in Figure 3: i) misalignment of two nearby deposited molecules along the direction of active dots axis. This would be caused by the imperfections of the gold grain, as shown in Figure 3(A) (a and a' are referred as two different positions in this direction). ii) Huge variation of the vertical positions among bis-ferrocene molecules, caused by the roughness of the gold substrate, as shown in Figure 3(B) (V and V' are referred as two different vertical positions). iii) Variation of the inter-molecule distance between two nearby molecules, in case of non identical number of hexane-dithiol elements between consecutive molecules, as shown in Figure 3(B) (d and d' identify two different distances); iv) Non ideal parallelism (tilted angle θ illustrated in Figure 3(A)) between two nearby molecules, due to the irregularity of the hexane-dithiol monolayer. All these mentioned defects might cause faults and mis-behaviors of the cells in the molecular QCA wire.

In this paper we explore the feasibility of using both oxidized and reduced form of the bis-ferrocene molecule to experimentally demonstrate QCA devices. This assessment is provided by a fault tolerance analysis based on the fabrication defects we were able to classify according to the abovementioned statements.

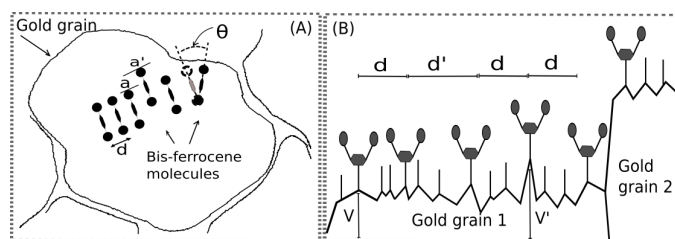


Fig. 3. Possible fabrication defects in the case of a QCA wire made of bis-ferrocene molecules. (A) Top view of a gold grain after molecule deposition: misalignment (a and a') and tilt angle (θ) defects are sketched. (B) Section of a bis-ferrocene SAM on gold: vertical shifts may occur due to the roughness inside a gold grain (V and V') or at the interface of two different grains. In addition, a different number of spacers (thiols) between two molecules may lead to a variation of the inter-molecule distance (d and d').

3. METHODOLOGY: MOSQUITO

Our goal in our study is to enlighten the electronic behavior of mQCA systems. In this specific work, for example, we aimed at assessing the behavior and the static energy of mQCA devices in presence of various fabrication defects. More in details we considered the technological defects caused by molecule displacement and analyzed a Molecule-Under-Test (MUT) misplaced with respect to a driver molecule. We observed the ability of the MUT to hold the information and to propagate it to a following molecule acting as a receiver. We also analyzed the electrostatic energy stored in the molecular system when the molecule's logic state is held or propagated along molecular QCA device.

Although this approach seems a simple procedure, if compared to what it is currently possible for standard technologies, as a matter of fact no tools currently allow to achieve these results. The approaches proposed in the literature are either non specific for actual molecular systems, like in the case of QCA designer [Walus][M.Momenzadeh and Lombardi 2005][Tahoori et al. 2004], or based on pure theoretical analysis. The only available source comes from chemistry, i.e. based on the solution of Schrodinger's equation. But the kind of information that can be obtained using this source, though very accurate, is far from what is necessary to determine, i.e. the correct behavior of a mQCA system observed adopting an electronic point of view.

In order to overcome the lack of tools suitable for this purpose we developed our own suite. We baptized it “**MoSQuiTo**” (*Molecular Simulator Quantum-dot cellular automata Torino*) [Pulimeno et al. 2014]. Its general claim is the capability to study a system of molecules and to analyze their potential for transferring information according to the QCA principle.

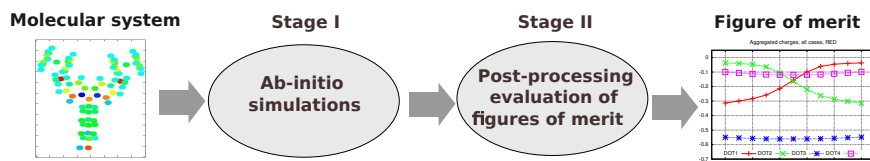


Fig. 4. MoSQuiTo: a two stage analysis transfers the general molecular system into device-level figures of merits from an electronic point of view.

This package is organized in two stages, as illustrated in the scheme of Figure 4. In **Stage I** accurate ab-initio simulations are performed based on the molecular system under different conditions as detailed herein. In **Stage II**, starting from Stage I data, electrostatic equations and models are set up. New figures of merits are defined to describe the QCA molecular system and to understand its potentials maintaining an

electronic point of view. The two stages are described in the following, while results for both stages are in section 4.

3.1. MoSQuiTo Stage I) Ab-initio simulations

The computations and evaluations of the electronic structure and properties we performed in this work are based on ab-initio simulations (see Figure 5(A)). They focus mainly on the laws of quantum mechanics and a set of physical constants. The analysis is highly accurate and, as a consequence, computationally intensive. In order to perform the fault analysis and energy evaluation of bisferrocene molecule as QCA device, a set of ab-initio simulations (Figure 5(A)) were performed. Simulation were iterated under different biasing conditions applied on the molecular system (Figure 5(B)), by defining suitable quantum chemistry methods and basis sets. Results are reported in section 4, while specific data are listed in tables III and IV at the bottom of the paper.

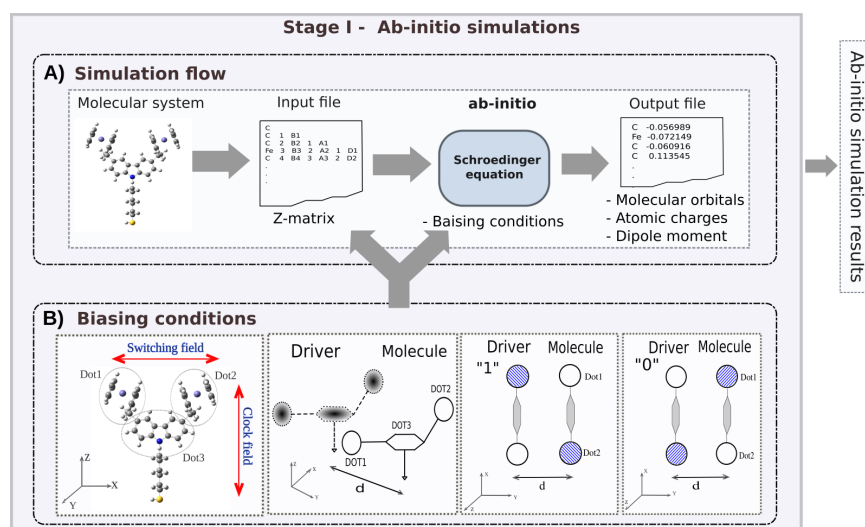


Fig. 5. “MoSQuiTo” methodology Stage I) Ab-initio simulations. (A) Simulation flow: from the chemical structure of the molecular system, its description in terms of *Z-matrix* (input file) to molecular system electrostatic quantities (output file). (B) The associated different biasing conditions: switching field and clock signal emulated by external electric field with proper directions, and model of driver-molecule system for analyzing the interaction between nearby molecules. The results of Stage I) will be the starting point of Stage II) (see Figure 6).

In particular, regarding the biasing conditions in ab-initio simulations [Pulimeno 2013], an uniform electric field parallel or vertical to the molecule axis was applied. This was done in order to emulate two external field. One is the switching field, which is responsible to force a logic state on a single molecule. The other is the clock signal, which can hinder or enhance the interaction between nearby molecules (Figure 5(B)). Additionally, concerning the interaction between nearby molecules, the methodology discussed here involves the simulations of a system as a complete QCA cell. It contains an ideal *Driver* represented by point charges located at the distance d from the target *Molecule*, as shown in Figure 5(B). The Driver plus molecule ensemble emulates the complete QCA cell. The point charge of the driver depends on the type of molecule (oxidized or reduced form). It is expected that due to the Coulomb repulsion, the target molecule re-arranges its logic state according to the logic state of the driver.

3.2. MoSQuiTo Stage II) Post-processing of data

Figure 6 gives an overview of the second stage of “MoSQuiTo” analysis. We start from the obtained accurate ab-initio simulation results in Stage-I, that are either chemical or physical properties of the molecule. We elaborate at this stage more usable quantities as defined in the following.

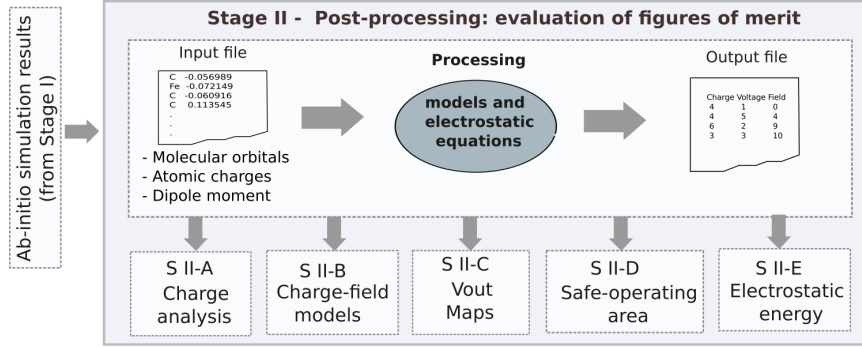


Fig. 6. Stage II) data post-processing: from ab-initio simulation results (performed in Stage I, see Figure 5) to device level figures of merits.

S II-A - Charge analysis. The **atomic charges** of the molecule in different operating conditions (ground state and biasing) are computed by means of ab-initio simulations (Stage I) using the Merz-Singh-Kollman (MK) approximation scheme (also called ESP) [Singh and Kollman 1984]. Furthermore, another new figure of merit defined as **aggregated charge** is computed in Stage II, basing on the given atomic charges of the molecule. The charge of the entire active dots and the central dot are computed by simply summing up the atomic charge of all the atoms that form the molecule for each of the sub-elements (Dots). The *aggregated charge* demonstrates the charge distribution inside a molecule from a macroscopic point of view. At the same time, it represents an easily readable quantity [Pulimeno et al. 2012][Pulimeno et al. 2013b].

S II-B - Charge-field. We start from the aggregated charges of the bis-ferrocene molecule obtained under different bias conditions. Then we compute the *electric field generated by the charge distribution* of the molecule at any specific working point through mathematical equations developed using Octave. For each charge q_i placed at (x_i, y_i, z_i) the generated electric field can be obtained by evaluating the force acting on a test charge in the position (x, y, z) . Considering a system of N point charges, the different forces related to the multiple charge distribution of the whole system affect the test charge. This effect could be summarized by defining a total force \vec{F}_{tot} and the total electric field $E_{tot}(x, y, z)$ calculated by

$$\vec{F}_{tot} = \sum_{i=1}^N \frac{1}{4\pi\epsilon_0} \frac{q_i \cdot q_t}{r_i^2} \cdot \hat{r} \quad E_{tot}(x, y, z) = \frac{\vec{F}_{tot}}{q_t} = \sum_{i=1}^N \frac{1}{4\pi\epsilon_0} \frac{q_i}{r_i^2} \cdot \hat{r} \quad (1)$$

Finally, considering a generic test charge placed at a generic point of the space (x, y, z) , the three component (E_x , E_y and E_z) of the electric field generated by a system of point charges are given by

$$E_x(x, y, z) = \sum_{i=1}^N E_{xi}(x, y, z) \quad E_y(x, y, z) = \sum_{i=1}^N E_{yi}(x, y, z) \quad E_z(x, y, z) = \sum_{i=1}^N E_{zi}(x, y, z) \quad (2)$$

S II-C V_{OUT} and V_{OUT} map. With a similar procedure the electric field generated by this system of charges (Figure 7(A)) at any point in the space that surrounds the molecule can be reckoned. As depicted in Figure 7(B), the electric field was “measured” putting an ideal receiver nearby the molecule with the ideal distance d (equal to the distance between two active dots of bis-ferrocene molecule) from it to form a squared cell. The *equivalent voltage at the receiver* (V_{OUT}) (Figure 7(C)) is computed by considering the component of the electric field parallel to the molecule and integrating it along the width of the molecule. In particular, for the map of V_{OUT} , a squared area

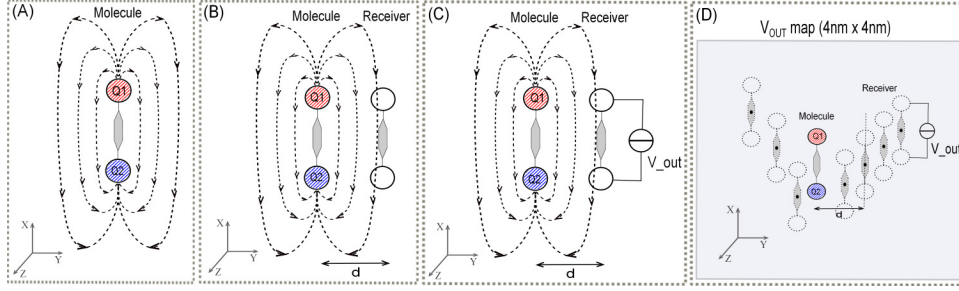


Fig. 7. (A) Generated electric field; (B-C) equivalent voltage at the receiver (V_{OUT}); (D) the V_{OUT} map.

(4nm × 4nm) of interest centered on the molecule is defined. As mentioned above, the electric field generated by the molecule charge distribution for two different logic states is adopted to calculate the corresponding equivalent voltage at the receiver (V_{OUT}). The V_{OUT} map records all the positions of the receiver while it moves around the molecule on the given area of interest and in each position the equivalent voltage is stored. Particularly, on the V_{OUT} map, the receiver position is shown plotting the midpoint of the ideal receiver (Figure 7(D)). It is important to notice that the map of V_{OUT} gives us a general idea about how the electric field distributes around the molecule and how the information could be propagated from the molecule to the receiver. Moreover, it is also fundamental to reckon the Safe-Operating-Area (SOA).

S II-D Safe-Operating-Area (SOA). In order to study the impact of the fabrication defects mentioned before, a Safe-Operating-Area (SOA), that highlights the fault tolerance of the mQCA, is defined as thoroughly discussed in the following.

SOA Methodology. Our analysis focuses on a system composed of three elements: an ideal emulated driver molecule, a bis-ferrocene Molecule-Under-Test (MUT) and an ideal receiver molecule. The aim is to evaluate the capability of the MUT to propagate the information in presence of fabrication defects. In particular, since we consider the bis-ferrocene in its oxidized form (or reduced form) with a positive net charge (negative net charge), in ab-initio simulations we emulated the ideal driver molecule as a polarized charge driver. The charge driver has two point charges. If one of these two point charges is forced equal to $+1q$ or $-1q$, it represents an oxidized or reduced bis-ferrocene molecule with a localized positive or negative charge, respectively. The driver was placed at a distance d equal to the distance between the two active dots (*Dot1* and *Dot2*) of the MUT, so that a 4 dots QCA squared cell was emulated. The localization of the point charge determines the logic state of the driver, as shown in Figure 8(A) and (D). In this way, we force a value at the input of the QCA wire and expect a consequent arrangement of charge inside the MUT (*Q1* and *Q2*), i.e. of its logic state (Figure 8(B) and (E)). Then, we considered an ideal receiver acting as the third molecule of this part of molecular wire, as shown in Figure 8(C) and (F). The electric field generated by

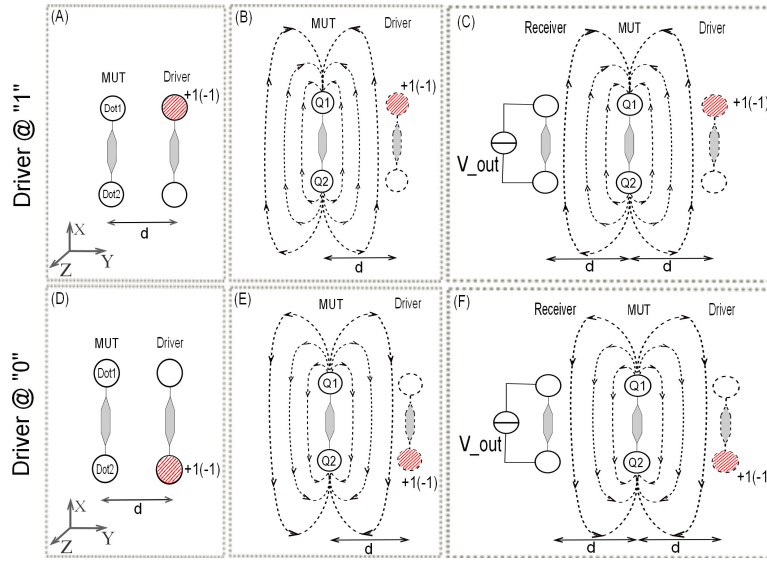


Fig. 8. Methodology scheme for the fault tolerance evaluation in case of bis-ferrocene molecular QCA wire: i) in the case of oxidized molecule, the point charge localized on the driver is $+1q$; ii) in the case of reduced molecule, the point charge localized on the driver is $-1q$.

the MUT is responsible of the state switching at the receiver, or, in other words, of the information propagation.

Defective conditions. Defects due to fabrication (mentioned in background section) are modeled varying the vertical position or tilted angle of the receiver with respect to the MUT as sketched in Figure 9. The misalignment between the receiver and the MUT that occurs along the active dots axis is defined as displacement at X-axis (δX in Figure 9(A)). The variation of the receiver-MUT distance with respect to the ideal inter-molecule distance d is called displacement at Y-axis (δY in Figure 9(B)). The vertical displacement of the receiver from the ideal position is defined as displacement at Z-axis (δZ in Figure 9(C)). At last, the non parallelism between the ideal receiver with respect to MUT is modeled as a tilted angle θ , as shown in Figure 9(D). As a starting point for the fault tolerance analysis, in this work, among all the above

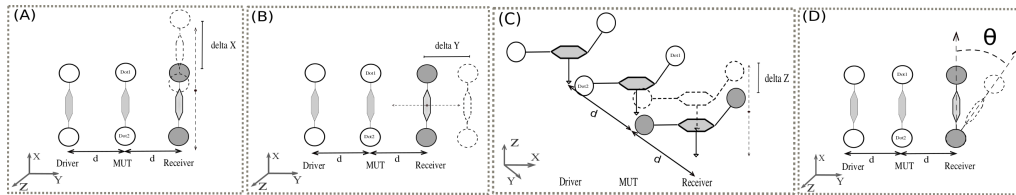


Fig. 9. Models applied to emulate all the four possible defects in the molecular QCA wire.

mentioned defects modeled in Figure 9, the last two of them were taken into consideration: i) the receiver moved perpendicularly with respect to the gold substrate (X-Y plane), where the ideal driver and MUT are located, resulting in a δZ along the Z-axis, as the case shown in Figure 9(C); ii) the ideal driver, the MUT as well as the receiver all located at the same plane (gold substrate), but there was a tilted angle θ of the receiver (as shown in Figure 9(D)). Therefore, by taking δZ and angle θ as

variables, a set of SOA plots could be generated demonstrating the fault tolerance of molecular QCA wire.

SOA calculation. In this work the driver was ideally aligned with MUT at distance d , i.e. they were on the same plane parallel with the gold substrate (X-Y plane). In sequence, then, the charge distribution of the MUT was obtained by means of interaction between ideal driver and MUT. Then the electric field generated and the equivalent voltage at the receiver was computed. This was repeated considering each case of fabrication defects related to the position of the receiver.

A *Safe-Operating-Area (SOA)* was finally calculated highlighting the working points of the receiver. *Working points* are defined as the points of localization of the non-ideal receiver in which the displacements or tilted angles of the receiver were tolerated and the information propagation through the molecular sequence was not compromised. In other words, these working points of SOA were plotted by classifying the *equivalent voltage at the receiver* and defining whether the receiver could still switch its logic state according to the logic state changing state of the MUT. Moreover, since each receiver displacement or tilted angle changed on a given area of interest (similar as the area of V_{OUT} map) centered on the MUT, different SOA could be drawn. Specifically, the electric field generated by the MUT in the two cases of the driver logic states was used to compute the *equivalent voltage at the receiver*, defined as V_{RX1} and V_{RX0} , for the driver logic state “1” and “0” respectively. Defining a set of threshold voltages (V_{th}) ranging from 0.1V to 1V, a generic point (x,y,z) of the area could be considered to be *safe* for any threshold voltage (V_{th}) that satisfied simultaneously the two following conditions:

$$V_{RX1}(x, y) > |V_{th}| \quad V_{RX0}(x, y) < -|V_{th}| \quad (3)$$

S II-E Electrostatic energy. The electrostatic potential energy is a potential energy (measured in Joules or eV) that results from conservative Coulomb forces. It is associated to the configuration of a particular set of point charges within a defined system. The electric potential energy of an object is the effect of two key elements: its own electric charge and its relative position to other electrically charged objects.

In our work, as shown in Figure 5(A), the ab-initio simulation results give the atomic charge distribution of the bis-ferrocene molecule in different biasing conditions. Once the charges of the molecule are in place, the persistence of the Coulomb force acts a key role. It makes the energy stored in the electrostatic field generated by the charge distribution potentially available whenever demanded for re-arranging its logic state or driving the nearby molecule (e.g. receiver). The communication based on QCA technology occurs without charge transportation. Consequently, in order to evaluate the electrostatic energy, we analyzed the potential energy stored in a molecular system. In particular, in terms of static charge distribution, each condition is associated to a charge distribution inside the molecule obtained by ab-initio simulation. The electrostatic energy depends only on the actual charge configuration. As a consequence, the associated energy is not affected by the sequence of the driver conditions. Thus, the switching is seen as a sequence of static conditions and not as a transient.

Specifically, for the bis-ferrocene molecule, instead of using the aggregated charge, we considered the atomic charge of all the 91 atoms in the molecule. The electrostatic energy stored in the whole system is calculated considering all the vectors \vec{r}_i and \vec{r}_j between q_i and q_j (where i, j run from 1 to 91), i.e. all the combinations among couples of atoms are considered). The electrostatic energy stored in the whole system is as defined in equation (4).

$$W_{tot} = \frac{1}{2} \cdot \frac{1}{4\pi\epsilon_0} \sum_{i=1}^{91} \sum_{j=1, j \neq i}^{91} \frac{q_i \cdot q_j}{|\vec{r}_i - \vec{r}_j|} \quad (4)$$

In other words, considering the atomic charges for the molecule at the equilibrium, the electrostatic energy can be seen as the work needed to bring static charges from infinity and assemble them in the required organization for QCA computation. When the molecule is not in the equilibrium condition, the total electrostatic energy changes. The difference with respect to the equilibrium can be defined as the energy which would be released to the molecule in order to obtain the encoding of logic states, as a consequence, letting the information to propagate through the molecular QCA devices.

4. RESULTS

In order to perform a fault tolerance analysis, we emulated the simultaneous concurrency of driver and receiver defects: we considered the charge distribution of the MUT for different driver charge configurations and we measured the effects on an ideal receiver. In particular, we firstly considered the dot axis of the receiver placed at the same height of the MUT dot axis. Then we introduced some defects in terms of vertical shift (delta Z) and tilted the dot axis (theta) with respect to the MUT. For all these cases, we moved the receiver on the whole XY plane and measured the equivalent voltage (defined as Vout) in order to emulate different receiver-molecule distances and dot misalignments.

According to the methodology described before, we chose a threshold value for the equivalent voltage at the receiver equal to $\pm 0.4V$. In Figure 10 the Vout maps for the oxidized molecule are shown: (A) and (B) refer to the two logic states of the driver when the free positive charge is completely localized on one of the dots and the charge difference between driver Dot1 and Dot2 is equal to 1 (ideal case of driver charge configuration); while (C) and (D) are related to the cases in which the driver dot charge difference is not the maximum value because the charge localization is lower (Dot1 charge = 0.3q and Dot2 charge = 0.7q, and vice versa for the opposite state). In all the figures the isolines related to $V_{out} = \pm 0.4V$ and $V_{out} = 0V$ are highlighted: in the ideal case of driver configuration, the isolines move to the left or to the right depending on the logic state of the driver, as well as in the case of lower charge difference. In the latter, the area included by the isolines of $V_{out} = \pm 0.4V$ is smaller, as well as the voltage inside those areas. This happens because a lower charge localization inside the driver has a weaker effect on the MUT and, as a consequence, the receiver-molecule interaction is less strong than in the ideal case.

The same results are obtained with the reduced form of the bisferrocene molecule (Figure 11). Even in this case, the ideal condition for the driver charge configuration (Figure 11(A) and (B)) leads to wider isolines and higher values of equivalent voltage at the receiver than in a non ideal case of driver configuration (Figure 11(C) and (D)).

In order to evaluate the fault tolerance of the bisferrocene molecule to some possible defects, we draw the Safe Operating Area (SOA). We consider the two logic states of the driver and highlight the receiver positions in which the binary encoding is preserved. The results are reported in Figure 12 for both oxidized and reduced form of the molecule. In particular, Figures 12(A) and (C) refer to the ideal case of driver configuration, while (B) and (D) to the lower charge localization. In the former two, the SOA are wider than in the latter two and this is a straightforward consequence of the Vout maps extent (Figures 10 and 11). The SOA are computed simply overlapping the Vout maps for the two logic states and selecting all the receiver positions in which the two voltages are opposite and their absolute values are higher than 0.4 V (see equation

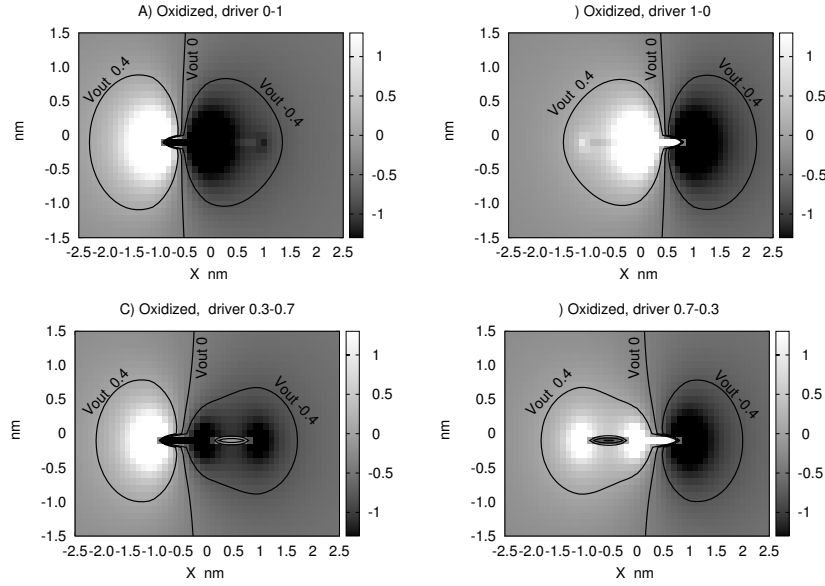


Fig. 10. Vout Maps for Oxidized Bisferrocene in different driver conditions. Isolines at $V_{out} = \pm 0.4V$ and $V_{out} = 0V$ are in evidence.

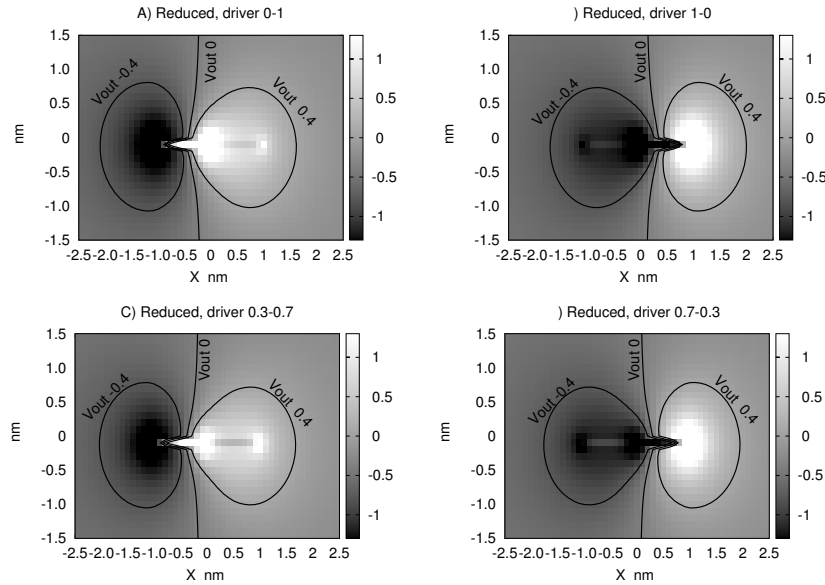


Fig. 11. Vout Maps for Reduced Bisferrocene in different driver conditions. Isolines at $V_{out} = \pm 0.4V$ and $V_{out} = 0V$ are in evidence.

(3) in Section 3.2). Moreover, comparing the performance of oxidized and reduced form in the ideal drive condition (Figures 12(A) and (C)), clearly the oxidized bisferrocene is more tolerant to the receiver defects in terms of dot misalignment and receiver-

molecule distance variations and, in addition, the values of the equivalent voltage at the receiver (gray scale) are higher than in the reduced bisferrocene.

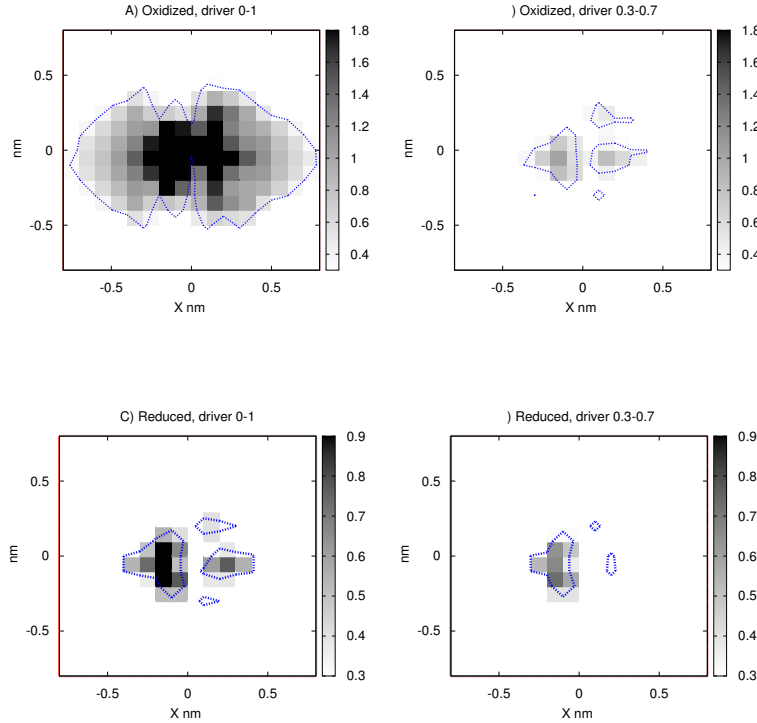


Fig. 12. Safe Operating Area Maps for Oxidized (A,B) and Reduced (C,D) Bisferrocene in different charge configurations of the driver dots.

To better evaluate the effect of non ideal charge localization inside the driver on the information propagation, we computed the extent of the SOA simply counting the receiver positions considered “safe” for a threshold voltage equal to $\pm 0.4V$. The results are given in \AA^2 , since the SOA is computed moving each time the receiver position of 1\AA along both the X and Y axis. Each safe point has then an extent of 1\AA^2 . Regarding the driver configuration, we started with the case in which the mobile charge is divided between the two dots (no logic state encoding). We then increased the charge of Dot1 while decreasing Dot2 charge and vice versa, defining the Dot1-Dot2 charge as the difference of charge between the two dots of the driver. In this way Dot1-Dot2 charge equal to 0 means no charge difference, while Dot1-Dot2 charge equal to 1 implies that the free mobile charge is completely localized in one of the two dots.

The results for both oxidized and reduced bisferrocene are collected in Table I and Table II, respectively, and they are also reported in Figure 13 for different cases of receiver defects, like vertical shifting (ΔZ) and molecule tilting (θ). In case of no deposition defects (continuous line in all the graphs), the SOA has the maximum extent. Decreasing the Dot1-Dot2 charge difference the SOA extent decreases as well, following a linear trend. In the case of a different height between receiver and MUT

Table I. Oxidized bisferrocene molecule: MUT energy and SOA extent as function of the driver configuration (*Dot1* and *Dot2* charges) and of the receiver defects (*theta* for tilting and *dZ* for vertical shift).

Driver		MUT	SOA extent [\AA^2]								
Dot1	Dot2	Energy	Theta				dZ				
[q]	[q]	[eV]	0deg	30deg	45deg	60deg	0.0nm	-0.3nm	-0.6nm	0.3nm	0.6nm
0.5	0.5	-18.936	0	0	0	0	0	0	0	0	0
0.6	0.4	-18.751	6	5	3	5	6	0	0	1	0
0.7	0.3	-18.648	25	8	10	9	25	11	0	7	0
0.8	0.2	-18.607	57	24	31	18	57	40	0	35	2
0.9	0.1	-18.560	73	39	40	24	73	49	12	53	7
1.0	0.0	-18.537	108	71	67	47	108	92	37	84	32

Table II. Reduced bisferrocene molecule: MUT energy and SOA extent as function of the driver configuration (*Dot1* and *Dot2* charges) and of the receiver defects (*theta* for tilting and *dZ* for vertical shift).

Driver		MUT	SOA extent [\AA^2]								
Dot1	Dot2	Energy	Theta				dZ				
[q]	[q]	[eV]	0deg	30deg	45deg	60deg	0.0nm	-0.3nm	-0.6nm	0.3nm	0.6nm
0.5	0.5	-23.467	0	0	0	0	0	0	0	0	0
0.6	0.4	-23.466	2	0	1	0	2	0	0	0	0
0.7	0.3	-23.451	11	3	3	0	11	0	0	2	0
0.8	0.2	-23.417	15	6	6	1	15	2	0	9	0
0.9	0.1	-23.373	21	7	8	2	21	4	0	18	0
1.0	0.0	-23.326	23	11	9	3	23	4	0	21	0

(Figures 13(A) and (C), see also Table I), the oxidized bisferrocene tolerates quite well vertical shifting in the range $\pm 0.3\text{nm}$, since the decrease of the SOA extent is not so huge. Further increase of the height difference between receiver and MUT leads to a drastic reduction of the area extent. On the other hand, the reduced bisferrocene seems to tolerate only vertical shifting in positive direction and not greater than $+0.3\text{nm}$. Regarding the effects of receiver tilting with respect to the MUT for both oxidized and reduced bisferrocene (Figures 13(B) and (D), see also Table I), a tilting angle within 45 degree leads to almost halve the SOA extent, while for higher values of tilting angle the SOA extent further decreases.

In Figure 14(B) the electrostatic energy variations are reported for the oxidized and reduced bisferrocene molecule. The driver configuration varies from the equilibrium condition (Dot1-Dot2 charge difference equals to 0 and so no logic state encoded) to one of the two binary states (Dot1-Dot2 charge difference equals to 1 and so mobile charge completely localized in one of the dots), gradually varying the charge of the two dots. The curves show the energy variation with respect to the equilibrium (Delta-Energy, top) as function of the driver configuration. They are obtained by simply subtracting the electrostatic energy of the molecule for a given driver configuration and the value corresponding to the driver at the equilibrium. For both reduced and oxidized molecule a larger charge difference on the driver corresponds to an higher energy for the molecule. As shown in Figure 14(B), the energy variation of the oxidized molecule are more pronounced than the reduced one. This is due to the charge distribution inside the molecule in presence of a driver. In particular the oxidized molecule shows a greater charge separation between the dots compared to the reduced one for the same driver configuration, as shown in Figure 14 (A). A good charge difference between the dots (ideally 1) is important to properly recognize the logic state of the device and for a better information propagation. For this reasons, the results of Figure 14(A) reveal that the performance in case of oxidized bisferrocene are better than for the reduced molecule. Moreover, the different condition in terms of driver configuration influences the trend of energy variation: a reduced Dot1-Dot2 charge difference on

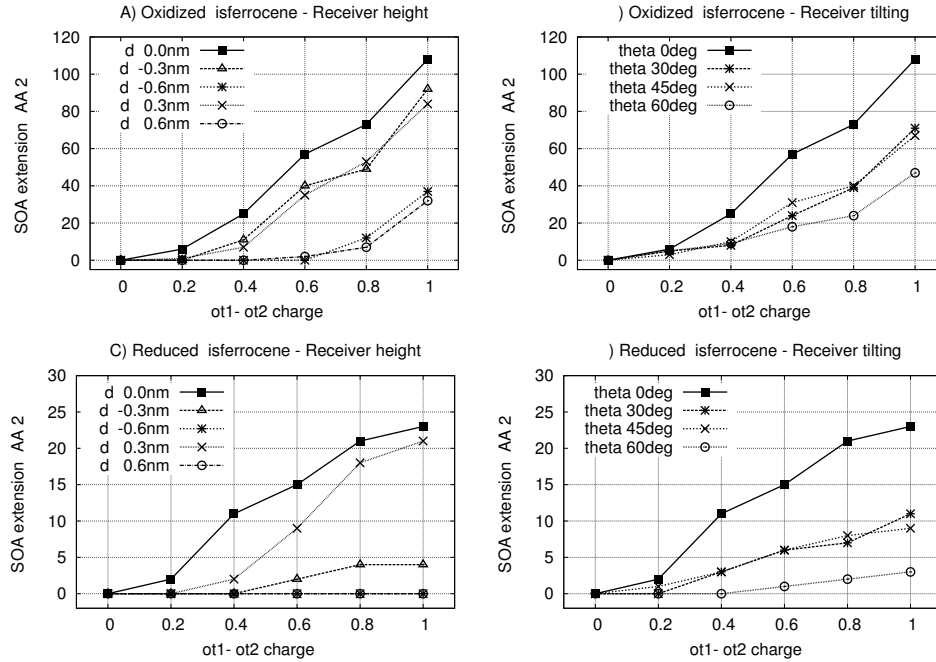


Fig. 13. SOA function of Dot1-Dot2 aggregated charge difference for Oxidized (A,B) and Reduced (C,D) molecule. Results obtained for different receiver height (A,C) and for different receiver tilt angle (B,D) are compared.

the driver corresponds to a low energy on the molecule. As a consequence, the energy involved in the driver-molecule interaction could be reduced decreasing the Dot1-Dot2 charge difference of the driver. This would imply a reduction of the power consumption during computation at the expenses of a still acceptable reduction of the SOA extent. For a complete electrostatic analysis, we also computed the *kink energy* [Lent et al. 2003] of both the oxidized and reduced bisferrocene for all the cases of driver configuration (Dot1-Dot2 charge difference). The results are shown at the bottom of Figure 14(B): in almost all the cases the kink energy is higher than the thermal voltage ($k_B T = 0.026 eV$), making the bisferrocene safe from thermodynamic mistake even for a reduced Dot1-Dot2 charge difference on the driver.

In order to evaluate the possibility to reduce the energy variation even when some fabrication defects occur, we computed the SOA extent. This was done as a function of the Delta-Energy of the molecule for different height (deltaZ) and tilting of the receiver (theta). The results are shown in Figure 15 for the oxidized bisferrocene and in Figure 16 for the reduced one. All the values are computed on the basis of the data in Table I and Table II for oxidized and reduced molecule, respectively.

Considering the oxidized bisferrocene, Figures 15(A) and (B) show the SOA extent trend as function of energy variation (absolute and percentage values, respectively) in case of different height between receiver and molecule (dZ). All the percentage values of SOA reduction are computed using as reference the ideal conditions for both driver configuration (maximum Dot1-Dot2 charge difference) and receiver defects (no vertical shifting and no tilting). The energy percentage variations are related to the maximum value (given by the maximum Dot1-Dot2 charge on the driver). In addition, in Figure 15(B) a dashed horizontal line indicates a 50% reduction of the SOA extent: considering

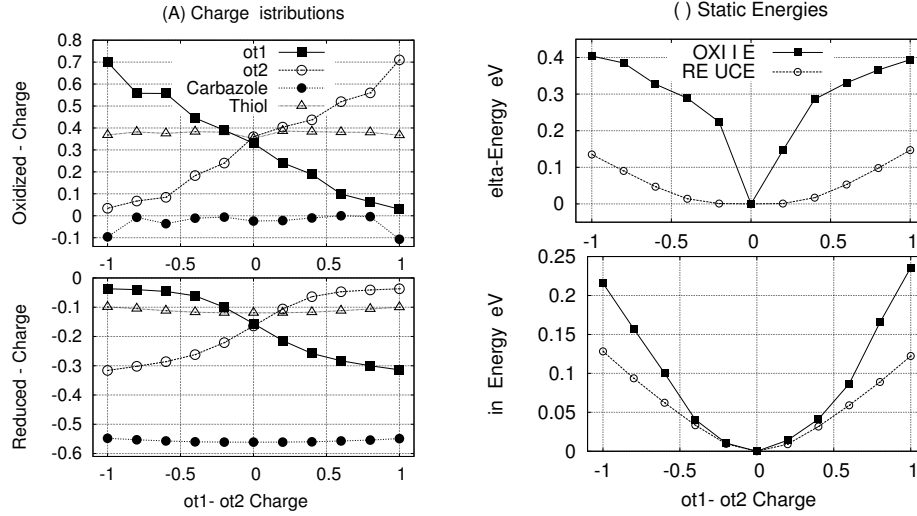


Fig. 14. (A) Charge distribution inside the oxidized (top) and reduced (bottom) bisferrocene for different driver configurations. (B) Delta-Energy (top) of both Oxidized (squares) and Reduced (circles) bisferrocene as a function of Dot1-Dot2 charge difference of the driver. Energy variation is computed w.r.t. the energy in the Dot1=Dot2 driver equilibrium state. The kink energy (bottom) as function of the driver configuration is also shown.

this value of reduction as a reasonable compromise, it is possible to reduce the energy of the driver down to 30% in case of no defects. On the contrary, in case of vertical shifting in the range $\pm 0.3\text{nm}$, only a 10% of energy reduction is allowed to keep the SOA reduction above 50%.

Regarding the tilting angle between receiver and molecule (θ), the results reported in Figures 15(C) and (D) show that it is not possible to reduce the energy in presence of receiver tilting since even a small decrease of the Delta-Energy leads to an abrupt reduction of the SOA extent for the values of angle considered.

For what concerns the reduced bisferrocene, the trend of SOA as a function of the energy variations is depicted in Figure 16. Even in this case some fabrication defects are considered and the results are given both in absolute and percentage values. In particular, Figures 16(A) and (B) show the trend of SOA in case of vertical shifting of the receiver (dZ): the results reveal that it is possible to strongly reduce the energy of the driver while keeping the SOA extent reduction over the 50%, even in case of $dZ = +0.3\text{nm}$. On the contrary, in presence of receiver tilting, it is not possible to further reduce the driver energy, since the SOA reduction is already higher than 50% for any case of tilting angle (θ). Moreover, in case of no vertical shifting and no tilting between receiver and MUT, if the energy of the driver is decreased down to 80%, the SOA reduction is still within 50%. However, it should be taken into account that the reference value (maximum SOA extent with maximum Dot1-Dot2 charge difference) is very small and this could limit the overall functionality of the QCA circuit in case of reduced bisferrocene molecules.

5. CONCLUSIONS AND FUTURE WORKS

We addressed two of the most important aspects of molecular QCA: I) the behavior of a mQCA device in presence of fabrication defects assessed in terms of correct information propagation capabilities; II) the electrostatic energy stored in the molecular QCA devices in different input and defects conditions, and, consequently, the correla-

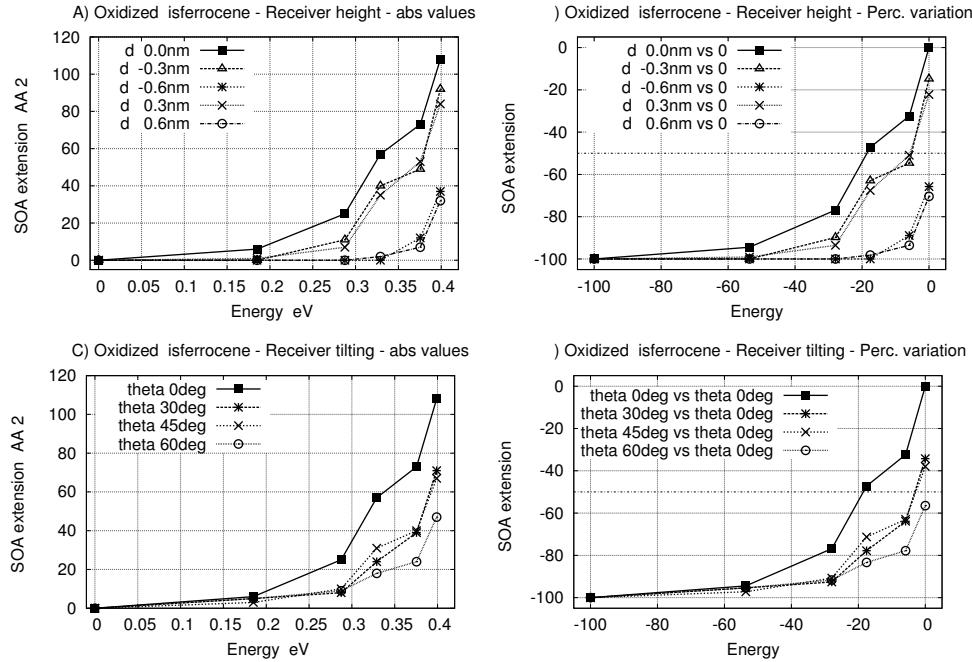


Fig. 15. SOA as a function of energy, for Oxidized molecule calculated in absolute (A,B) and percentage (C,D) value. Results obtained for different receiver height (A,C) and for different receiver tilt angle (B,D) are compared.

tion between energy and correct information propagation. In particular, our analysis focused on both the oxidized and the reduced form of the bis-ferrocene. The key point at the basis of these achievements was the development of a systematic approach for the quantitative evaluation of the characterization of a mQCA device from an electronic point of view (MoSQUiTo).

The results obtained reveal a few important key-points. A) The oxidized form shows better performance and robustness than the reduced one. Considering the fabrication of a QCA wire with oxidized bis-ferrocenes and defined a reasonable value of tolerance reduction (given by the SOA extension), B) it is possible to reduce the energy at the input even in presence of some fabrication defects. This means that an improvement at the technological level performed to fit the constraints given by the SOA extension could lead to a further reduction of the power consumption. C) the results obtained represent an important feedback for the molecular QCA prototyping and circuit fabrication. Finally, D) the methodology is general and can be applied to other molecules proposed as candidates for a computing system based on the mQCA principle.

APPENDIX

Atom	Driver configurations [Dot1/Dot2]											
	1.0/0.0	0.9/0.1	0.8/0.2	0.7/0.3	0.6/0.4	0.5/0.5	0.4/0.6	0.3/0.7	0.2/0.8	0.1/0.9	0.0/1.0	
C	-0.105	-0.104	-0.097	-0.094	-0.090	-0.089	-0.080	-0.076	-0.070	-0.068	-0.064	
C	-0.154	-0.152	-0.145	-0.143	-0.138	-0.137	-0.125	-0.121	-0.118	-0.112	-0.111	
C	-0.113	-0.111	-0.102	-0.099	-0.094	-0.094	-0.080	-0.075	-0.071	-0.065	-0.063	
C	-0.140	-0.138	-0.130	-0.126	-0.121	-0.118	-0.111	-0.106	-0.098	-0.096	-0.091	
C	-0.116	-0.114	-0.108	-0.105	-0.102	-0.100	-0.094	-0.091	-0.084	-0.084	-0.079	

Fe	-0.003	0.005	-0.019	-0.010	-0.024	0.030	-0.034	-0.028	-0.030	-0.032	0.063
C	-0.205	-0.203	-0.191	-0.189	-0.183	-0.179	-0.167	-0.161	-0.154	-0.149	-0.141
C	0.038	0.044	0.051	0.056	0.062	0.063	0.079	0.085	0.092	0.098	0.106
C	-0.208	-0.207	-0.198	-0.195	-0.190	-0.190	-0.178	-0.174	-0.169	-0.166	-0.168
C	-0.110	-0.109	-0.100	-0.097	-0.092	-0.090	-0.077	-0.073	-0.065	-0.061	-0.054
C	-0.207	-0.206	-0.197	-0.195	-0.190	-0.190	-0.181	-0.178	-0.170	-0.171	-0.171
C	0.092	0.087	0.083	0.076	0.070	0.068	0.061	0.058	0.045	0.046	0.039
C	-0.474	-0.469	-0.458	-0.453	-0.444	-0.442	-0.424	-0.417	-0.409	-0.402	-0.396
C	0.103	0.124	0.117	0.118	0.111	0.111	0.102	0.098	0.101	0.094	0.080
C	-0.203	-0.197	-0.199	-0.200	-0.201	-0.199	-0.202	-0.202	-0.205	-0.205	-0.206
C	-0.092	-0.084	-0.079	-0.077	-0.074	-0.074	-0.065	-0.063	-0.057	-0.056	-0.062
C	0.390	0.388	0.390	0.388	0.386	0.392	0.384	0.385	0.382	0.383	0.386
C	-0.346	-0.326	-0.326	-0.324	-0.326	-0.326	-0.321	-0.321	-0.318	-0.318	-0.331
C	-0.223	-0.227	-0.229	-0.229	-0.229	-0.231	-0.229	-0.229	-0.232	-0.230	-0.228
C	-0.069	-0.060	-0.067	-0.068	-0.073	-0.072	-0.080	-0.082	-0.087	-0.089	-0.095
C	0.390	0.386	0.390	0.388	0.389	0.393	0.390	0.392	0.390	0.392	0.394
N	-0.485	-0.444	-0.449	-0.446	-0.450	-0.449	-0.445	-0.447	-0.443	-0.445	-0.476
C	-0.207	-0.206	-0.204	-0.203	-0.202	-0.202	-0.201	-0.201	-0.198	-0.198	-0.203
C	0.080	0.102	0.098	0.102	0.107	0.100	0.121	0.121	0.127	0.127	0.111
C	-0.235	-0.240	-0.236	-0.236	-0.236	-0.237	-0.236	-0.236	-0.235	-0.235	-0.232
C	-0.330	-0.313	-0.316	-0.316	-0.319	-0.320	-0.319	-0.320	-0.320	-0.321	-0.336
C	0.038	0.040	0.054	0.057	0.059	0.069	0.069	0.075	0.080	0.086	0.091
C	-0.393	-0.400	-0.408	-0.414	-0.424	-0.425	-0.444	-0.450	-0.460	-0.465	-0.471
C	0.107	0.097	0.090	0.085	0.080	0.079	0.063	0.057	0.050	0.045	0.041
C	-0.170	-0.167	-0.172	-0.175	-0.183	-0.178	-0.194	-0.197	-0.205	-0.207	-0.209
C	-0.053	-0.060	-0.069	-0.073	-0.078	-0.076	-0.095	-0.098	-0.106	-0.109	-0.110
C	-0.169	-0.166	-0.174	-0.177	-0.182	-0.180	-0.190	-0.193	-0.201	-0.203	-0.205
C	-0.142	-0.150	-0.158	-0.164	-0.171	-0.166	-0.188	-0.191	-0.202	-0.205	-0.207
Fe	0.093	-0.031	-0.025	-0.028	0.010	-0.049	0.005	-0.010	0.003	0.006	0.000
C	-0.087	-0.090	-0.097	-0.100	-0.103	-0.103	-0.112	-0.115	-0.120	-0.123	-0.125
C	-0.069	-0.072	-0.079	-0.082	-0.086	-0.086	-0.097	-0.100	-0.107	-0.109	-0.111
C	-0.112	-0.115	-0.119	-0.122	-0.128	-0.127	-0.140	-0.144	-0.150	-0.153	-0.155
C	-0.064	-0.068	-0.072	-0.076	-0.084	-0.082	-0.098	-0.101	-0.109	-0.112	-0.114
C	-0.088	-0.091	-0.099	-0.103	-0.108	-0.109	-0.119	-0.123	-0.131	-0.135	-0.137
H	0.076	0.076	0.076	0.078	0.078	0.079	0.078	0.078	0.081	0.080	0.082
H	0.137	0.137	0.131	0.130	0.127	0.127	0.119	0.116	0.114	0.111	0.109
H	0.133	0.133	0.134	0.134	0.135	0.135	0.136	0.136	0.138	0.138	0.138
H	0.106	0.106	0.105	0.105	0.105	0.105	0.104	0.103	0.103	0.102	0.102
H	0.108	0.110	0.112	0.115	0.119	0.115	0.128	0.129	0.134	0.135	0.136
H	0.101	0.102	0.102	0.102	0.103	0.103	0.104	0.105	0.105	0.105	0.105
H	0.137	0.137	0.136	0.136	0.135	0.136	0.134	0.134	0.132	0.132	0.132
H	0.151	0.151	0.150	0.149	0.148	0.149	0.145	0.145	0.143	0.143	0.142
H	0.160	0.160	0.158	0.158	0.157	0.158	0.155	0.154	0.153	0.152	0.152
H	0.147	0.146	0.143	0.142	0.141	0.141	0.138	0.137	0.135	0.134	0.133
H	0.146	0.144	0.141	0.139	0.135	0.135	0.128	0.126	0.123	0.121	0.119
H	0.151	0.150	0.148	0.147	0.145	0.145	0.140	0.139	0.136	0.135	0.135
H	0.158	0.157	0.155	0.154	0.154	0.154	0.151	0.151	0.149	0.149	0.149
H	0.164	0.164	0.161	0.160	0.159	0.158	0.157	0.155	0.154	0.152	0.152
H	0.176	0.174	0.173	0.172	0.170	0.170	0.166	0.165	0.163	0.162	0.161
H	0.156	0.157	0.156	0.156	0.155	0.155	0.153	0.153	0.152	0.151	0.151
H	0.148	0.149	0.150	0.150	0.151	0.152	0.154	0.154	0.156	0.156	0.157
H	0.151	0.151	0.153	0.153	0.154	0.153	0.156	0.156	0.157	0.157	0.157
H	0.162	0.162	0.165	0.166	0.167	0.167	0.171	0.172	0.174	0.176	0.177
H	0.151	0.152	0.154	0.155	0.157	0.157	0.159	0.160	0.163	0.163	0.164
H	0.138	0.138	0.140	0.141	0.142	0.141	0.145	0.146	0.146	0.147	0.147
H	0.130	0.131	0.134	0.135	0.136	0.136	0.141	0.142	0.144	0.146	0.147
H	0.119	0.120	0.124	0.126	0.129	0.130	0.136	0.138	0.141	0.144	0.146
H	0.132	0.133	0.136	0.137	0.138	0.139	0.140	0.141	0.144	0.144	0.146
H	0.151	0.151	0.153	0.153	0.154	0.154	0.156	0.156	0.158	0.158	0.158
H	0.173	0.171	0.170	0.170	0.170	0.169	0.169	0.168	0.168	0.167	0.166

H	0.157	0.157	0.157	0.157	0.157	0.157	0.157	0.157	0.158	0.157	0.158
H	0.220	0.218	0.218	0.218	0.218	0.218	0.218	0.218	0.218	0.218	0.220
H	0.222	0.220	0.219	0.219	0.219	0.219	0.219	0.219	0.219	0.219	0.221
H	0.159	0.159	0.158	0.158	0.159	0.157	0.159	0.158	0.158	0.158	0.158
H	0.168	0.169	0.168	0.169	0.170	0.168	0.172	0.172	0.172	0.173	0.174
H	0.082	0.081	0.077	0.077	0.078	0.075	0.078	0.077	0.076	0.076	0.075
C	-0.139	-0.145	-0.143	-0.144	-0.144	-0.144	-0.145	-0.144	-0.145	-0.144	-0.140
C	0.091	0.094	0.096	0.095	0.094	0.094	0.094	0.095	0.094	0.095	0.092
H	0.125	0.126	0.126	0.126	0.127	0.126	0.128	0.127	0.129	0.128	0.127
H	0.130	0.132	0.130	0.131	0.131	0.130	0.130	0.130	0.130	0.129	0.128
H	0.002	0.001	0.001	0.001	0.001	0.000	0.000	0.000	0.000	0.000	-0.000
H	0.015	0.015	0.015	0.015	0.016	0.016	0.016	0.016	0.017	0.017	0.017
C	0.242	0.242	0.241	0.242	0.242	0.238	0.242	0.242	0.243	0.242	0.241
H	-0.049	-0.049	-0.049	-0.049	-0.049	-0.049	-0.049	-0.049	-0.050	-0.049	-0.050
H	-0.046	-0.046	-0.046	-0.046	-0.046	-0.046	-0.045	-0.045	-0.045	-0.045	-0.046
C	-0.016	-0.021	-0.021	-0.021	-0.019	-0.016	-0.020	-0.021	-0.021	-0.021	-0.017
C	0.307	0.304	0.305	0.305	0.305	0.310	0.304	0.305	0.304	0.304	0.307
H	-0.065	-0.064	-0.064	-0.064	-0.064	-0.066	-0.064	-0.064	-0.064	-0.064	-0.066
H	-0.034	-0.033	-0.033	-0.033	-0.033	-0.034	-0.032	-0.032	-0.032	-0.032	-0.033
H	-0.093	-0.092	-0.092	-0.092	-0.092	-0.094	-0.092	-0.092	-0.092	-0.092	-0.093
H	-0.059	-0.058	-0.058	-0.058	-0.058	-0.060	-0.058	-0.058	-0.057	-0.057	-0.059
C	0.045	0.048	0.050	0.050	0.047	0.042	0.048	0.050	0.048	0.048	0.045
H	0.006	0.007	0.006	0.006	0.006	0.005	0.006	0.006	0.006	0.006	0.005
H	0.130	0.128	0.127	0.128	0.129	0.131	0.129	0.128	0.129	0.129	0.130
S	-0.544	-0.530	-0.527	-0.527	-0.534	-0.551	-0.530	-0.527	-0.530	-0.529	-0.542
H	0.319	0.318	0.317	0.317	0.318	0.319	0.318	0.317	0.318	0.318	0.318

Table III: Oxidized bisferrocene molecule: MUT atomic charges [q] as function of the driver configuration (*Dot1* and *Dot2* charges).

Atom	Driver configurations [Dot1/Dot2]											
	-1.0/0.0	-0.9/-0.1	-0.8/-0.2	-0.7/-0.3	-0.6/-0.4	-0.5/-0.5	-0.4/-0.6	-0.3/-0.7	-0.2/-0.8	-0.1/-0.9	0.0/-1.0	
C	-0.157	-0.157	-0.158	-0.160	-0.167	-0.178	-0.188	-0.197	-0.201	-0.204	-0.206	
C	-0.194	-0.194	-0.195	-0.195	-0.197	-0.199	-0.201	-0.202	-0.203	-0.204	-0.204	
C	-0.121	-0.122	-0.122	-0.124	-0.129	-0.136	-0.143	-0.148	-0.151	-0.153	-0.155	
C	-0.156	-0.158	-0.159	-0.162	-0.168	-0.175	-0.183	-0.190	-0.195	-0.198	-0.201	
C	-0.132	-0.133	-0.133	-0.134	-0.134	-0.135	-0.136	-0.136	-0.136	-0.136	-0.136	
Fe	0.048	0.048	0.049	0.052	0.062	0.078	0.094	0.106	0.112	0.116	0.119	
C	-0.149	-0.148	-0.148	-0.149	-0.155	-0.164	-0.174	-0.181	-0.185	-0.187	-0.188	
C	0.003	0.002	0.000	-0.001	-0.007	-0.014	-0.022	-0.028	-0.031	-0.032	-0.034	
C	-0.189	-0.189	-0.188	-0.189	-0.190	-0.192	-0.194	-0.196	-0.197	-0.198	-0.199	
C	-0.106	-0.105	-0.104	-0.106	-0.113	-0.125	-0.136	-0.144	-0.148	-0.150	-0.151	
C	-0.198	-0.198	-0.198	-0.199	-0.200	-0.201	-0.203	-0.204	-0.204	-0.204	-0.204	
C	0.150	0.154	0.159	0.163	0.167	0.172	0.177	0.182	0.186	0.189	0.193	
C	-0.461	-0.463	-0.466	-0.470	-0.476	-0.484	-0.493	-0.500	-0.505	-0.509	-0.513	
C	0.072	0.070	0.069	0.068	0.070	0.074	0.077	0.079	0.080	0.079	0.079	
C	-0.219	-0.219	-0.219	-0.218	-0.216	-0.215	-0.213	-0.211	-0.210	-0.209	-0.208	
C	-0.102	-0.102	-0.103	-0.105	-0.108	-0.113	-0.117	-0.120	-0.121	-0.121	-0.120	
C	0.465	0.466	0.468	0.470	0.471	0.472	0.473	0.474	0.473	0.472	0.470	
C	-0.400	-0.400	-0.400	-0.400	-0.401	-0.402	-0.403	-0.404	-0.404	-0.404	-0.403	
C	-0.276	-0.277	-0.278	-0.279	-0.279	-0.279	-0.279	-0.278	-0.278	-0.278	-0.278	
C	-0.125	-0.126	-0.127	-0.126	-0.123	-0.119	-0.114	-0.111	-0.109	-0.108	-0.107	
C	0.473	0.475	0.477	0.478	0.477	0.476	0.475	0.474	0.472	0.470	0.469	
N	-0.645	-0.648	-0.650	-0.652	-0.653	-0.653	-0.653	-0.652	-0.650	-0.648	-0.645	
C	-0.209	-0.210	-0.211	-0.212	-0.213	-0.215	-0.217	-0.218	-0.219	-0.219	-0.220	
C	0.082	0.082	0.082	0.082	0.080	0.077	0.073	0.070	0.071	0.072	0.074	
C	-0.286	-0.286	-0.286	-0.286	-0.286	-0.287	-0.287	-0.287	-0.286	-0.285	-0.283	

C	-0.398	-0.399	-0.399	-0.399	-0.398	-0.397	-0.396	-0.395	-0.395	-0.395	-0.395
C	0.192	0.189	0.185	0.182	0.177	0.172	0.168	0.163	0.159	0.155	0.151
C	-0.508	-0.504	-0.500	-0.496	-0.489	-0.481	-0.472	-0.466	-0.462	-0.459	-0.457
C	-0.032	-0.030	-0.029	-0.026	-0.021	-0.013	-0.005	-0.000	0.002	0.004	0.005
C	-0.200	-0.199	-0.198	-0.197	-0.195	-0.193	-0.191	-0.189	-0.189	-0.189	-0.189
C	-0.151	-0.150	-0.148	-0.145	-0.137	-0.126	-0.115	-0.107	-0.105	-0.105	-0.107
C	-0.201	-0.201	-0.201	-0.201	-0.200	-0.199	-0.197	-0.196	-0.195	-0.195	-0.195
C	-0.191	-0.190	-0.188	-0.185	-0.178	-0.168	-0.159	-0.153	-0.151	-0.151	-0.152
Fe	0.120	0.118	0.114	0.109	0.097	0.082	0.065	0.054	0.050	0.049	0.050
C	-0.147	-0.147	-0.147	-0.147	-0.146	-0.146	-0.145	-0.144	-0.144	-0.143	-0.143
C	-0.213	-0.211	-0.208	-0.204	-0.196	-0.185	-0.174	-0.166	-0.164	-0.163	-0.163
C	-0.205	-0.205	-0.204	-0.203	-0.202	-0.200	-0.198	-0.196	-0.196	-0.195	-0.195
C	-0.156	-0.155	-0.152	-0.150	-0.145	-0.138	-0.131	-0.126	-0.124	-0.123	-0.123
C	-0.197	-0.194	-0.191	-0.186	-0.180	-0.172	-0.164	-0.159	-0.155	-0.154	-0.152
H	0.045	0.044	0.043	0.043	0.042	0.041	0.041	0.040	0.039	0.039	0.038
H	0.119	0.118	0.118	0.118	0.119	0.122	0.126	0.128	0.129	0.130	0.130
H	0.123	0.124	0.124	0.124	0.124	0.123	0.123	0.123	0.122	0.122	0.122
H	0.119	0.119	0.119	0.119	0.119	0.120	0.120	0.121	0.121	0.121	0.121
H	0.128	0.127	0.127	0.126	0.124	0.121	0.118	0.116	0.115	0.116	0.117
H	0.120	0.120	0.120	0.120	0.119	0.119	0.118	0.118	0.118	0.118	0.118
H	0.121	0.121	0.121	0.122	0.122	0.122	0.123	0.123	0.123	0.123	0.123
H	0.131	0.131	0.131	0.131	0.131	0.131	0.131	0.131	0.131	0.131	0.130
H	0.138	0.138	0.138	0.139	0.139	0.141	0.142	0.143	0.143	0.143	0.142
H	0.123	0.123	0.124	0.124	0.125	0.127	0.128	0.129	0.129	0.129	0.129
H	0.128	0.129	0.131	0.132	0.134	0.137	0.139	0.141	0.143	0.144	0.145
H	0.120	0.121	0.121	0.122	0.124	0.126	0.129	0.130	0.131	0.131	0.131
H	0.121	0.121	0.121	0.122	0.123	0.124	0.125	0.126	0.127	0.127	0.126
H	0.144	0.145	0.146	0.147	0.149	0.150	0.151	0.152	0.153	0.154	0.154
H	0.138	0.138	0.139	0.139	0.141	0.143	0.145	0.147	0.147	0.147	0.148
H	0.121	0.122	0.122	0.122	0.122	0.122	0.122	0.122	0.122	0.122	0.122
H	0.126	0.127	0.127	0.126	0.126	0.124	0.123	0.122	0.121	0.121	0.121
H	0.122	0.122	0.122	0.122	0.122	0.122	0.122	0.122	0.122	0.122	0.122
H	0.148	0.148	0.148	0.148	0.146	0.144	0.142	0.140	0.140	0.139	0.139
H	0.154	0.153	0.152	0.151	0.150	0.149	0.148	0.147	0.146	0.145	0.144
H	0.126	0.126	0.126	0.126	0.126	0.126	0.126	0.126	0.126	0.126	0.126
H	0.126	0.126	0.125	0.125	0.123	0.121	0.119	0.117	0.116	0.115	0.114
H	0.145	0.144	0.143	0.141	0.139	0.137	0.134	0.132	0.130	0.129	0.127
H	0.128	0.128	0.128	0.128	0.127	0.126	0.124	0.123	0.123	0.122	0.122
H	0.141	0.141	0.141	0.141	0.141	0.139	0.138	0.137	0.136	0.136	0.136
H	0.165	0.165	0.164	0.164	0.163	0.163	0.163	0.163	0.163	0.163	0.163
H	0.126	0.126	0.126	0.125	0.125	0.125	0.125	0.125	0.125	0.125	0.125
H	0.218	0.219	0.219	0.219	0.219	0.219	0.219	0.219	0.218	0.218	0.218
H	0.219	0.219	0.220	0.220	0.220	0.220	0.220	0.220	0.220	0.220	0.220
H	0.126	0.126	0.127	0.127	0.127	0.127	0.127	0.127	0.127	0.127	0.128
H	0.164	0.164	0.164	0.164	0.164	0.164	0.164	0.165	0.165	0.166	0.166
H	0.037	0.038	0.038	0.039	0.039	0.040	0.041	0.041	0.042	0.043	0.043
C	-0.197	-0.199	-0.200	-0.201	-0.201	-0.201	-0.201	-0.201	-0.200	-0.199	-0.198
C	0.261	0.263	0.265	0.267	0.267	0.267	0.267	0.267	0.266	0.266	0.261
H	0.003	0.001	0.000	-0.001	-0.001	-0.002	-0.002	-0.002	-0.000	0.000	0.002
H	0.006	0.004	0.002	0.001	0.001	0.001	0.001	0.002	0.003	0.005	0.006
H	-0.070	-0.071	-0.071	-0.072	-0.072	-0.072	-0.071	-0.071	-0.070	-0.068	-0.067
H	-0.050	-0.051	-0.052	-0.054	-0.054	-0.054	-0.055	-0.055	-0.054	-0.054	-0.053
C	0.213	0.213	0.213	0.213	0.213	0.213	0.213	0.213	0.213	0.213	0.213
H	-0.092	-0.093	-0.093	-0.094	-0.094	-0.094	-0.094	-0.094	-0.094	-0.093	-0.093
H	-0.089	-0.089	-0.089	-0.090	-0.090	-0.090	-0.090	-0.090	-0.089	-0.089	-0.088
C	0.050	0.052	0.053	0.054	0.055	0.055	0.055	0.054	0.053	0.052	0.051
C	0.374	0.374	0.374	0.375	0.375	0.375	0.375	0.375	0.374	0.374	0.373
H	-0.108	-0.109	-0.110	-0.110	-0.111	-0.111	-0.110	-0.110	-0.110	-0.109	-0.109
H	-0.073	-0.073	-0.074	-0.075	-0.075	-0.075	-0.075	-0.075	-0.074	-0.074	-0.073
H	-0.124	-0.124	-0.124	-0.124	-0.124	-0.124	-0.124	-0.124	-0.124	-0.124	-0.123

H	-0.087	-0.087	-0.087	-0.088	-0.088	-0.088	-0.088	-0.088	-0.088	-0.087	-0.087
C	0.096	0.096	0.095	0.095	0.095	0.095	0.095	0.095	0.095	0.095	0.096
H	-0.014	-0.014	-0.014	-0.014	-0.014	-0.014	-0.013	-0.013	-0.013	-0.013	-0.013
H	0.113	0.113	0.113	0.113	0.113	0.113	0.113	0.113	0.113	0.112	0.112
S	-0.629	-0.630	-0.630	-0.631	-0.631	-0.631	-0.631	-0.631	-0.631	-0.630	-0.630
H	0.319	0.319	0.319	0.319	0.320	0.320	0.320	0.320	0.320	0.320	0.320

Table IV: Reduced bisferrocene molecule: MUT atomic charges [q] as function of the driver configuration (*Dot1* and *Dot2* charges).

REFERENCES

- V. Arima, M. Iurlo, L. Zoli, S. Kumar, M. Piacenza, F. Della Sala, F. Martino, G. Maruccio, R. Rinaldi, F. Paolucci, M. Marcaccio, P.G. Cozzi, and A.P. Bramanti. 2012. Toward quantum-dot cellular automata units: thiolated-carbazole linked bis-ferrocene. *Nanoscale* 4 (2012), 813–823.
- M. Awais, M. Vacca, M. Graziano, and G. Masera. 2012. FFT implementation using QCA. *2012 19th IEEE International Conference on Electronics, Circuits, and Systems, ICECS 2012* (2012), 741–744.
- M. Awais, M. Vacca, M. Graziano, M. Ruoch, and G. Masera. 2013. Quantum Dot Cellular Automata Check Node Implementation for LDPC Decoders. *IEEE TRANSACTIONS ON NANOTECHNOLOGY* 12 (2013), 368–377.
- Enrique P. Blair, Eric Yost, and Craig S. Lent. 2009. Power dissipation in clocking wires for clocked molecular quantum-dot cellular automata. *Journal of Computational Electronics - Springer* (2009). DOI: <http://dx.doi.org/10.1007/s10825-009-0304-0>
- M. R. Casu, M. Graziano, G. Masera, G. Piccinini, and M. Zamboni. 2004. An Electromigration and Thermal Model of Power Wires for a Priori High-Level Reliability Prediction. *IEEE TRANSACTIONS ON VERY LARGE SCALE INTEGRATION (VLSI) SYSTEMS* 12 (2004), 349–358.
- A. Chiolerio, P. Allia, and M. Graziano. 2012. Magnetic dipolar coupling and collective effects for binary information codification in cost-effective logic devices. *Journal of Magnetism and Magnetic Materials* 324 (2012), 3006–3012.
- O. Fenwick, L. Bozec, D. Credgington, A. Hammiche, G.M. Lazzerini, Y.R. Silberberg, and F. Cacialli. 2009. Thermochemical nanopatterning of organic semiconductors. *Nature Nanotechnology* 4(10) (2009), 664–668.
- M. Graziano, S. Frache, and M. Zamboni. 2013. A Hardware Viewpoint on Biosequence Analysis: What's Next? *ACM Journal on Emerging Technologies in Computing Systems* 9, 4 (Nov. 2013).
- M. Graziano, M. Vacca, A. Chiolerio, and M. Zamboni. 2011. A NCL-HDL Snake-Clock Based Magnetic QCA Architecture. *IEEE Transaction on Nanotechnology* 10, 5 (Sept. 2011), 1141–1149.
- A. Imre, G. Csabaa, G.H. Bernstein, W. Porod, and V. Metlushkob. 2003. Investigation of shape-dependent switching of coupled nanomagnets. *Superlattices and Microstructures* 34 (2003), 513–518.
- J.Jiao, G.J. Long, F. Grandjean, A.M. Beatty, and T.P.Fehlner. 2003. Building Blocks for the Molecular Expression of Quantum Cellular Automata. Isolation and Characterization of a Covalently Bonded Square Array of Two Ferrocenium and Two Ferrocene Complexes. *Journal of American Chemical Society, Communication* 125 (2003).
- C.S. Lent, B. Isaksen, and M. Lieberman. 2003. Molecular Quantum-Dot Cellular Automata. *Journal of American Chemical Society* 125 (2003), 1056–1063.
- C.S. Lent, P.D. Tougaw, W. Porod, and G. Bernstein. 1993. Quantum cellular automata. *Nanotechnology* 4 (1993), 49–57.
- Z. Li, A. M. Beatty, and T. P. Fehlner. 2003. Molecular QCA Cell: Structure and functionalization of an Unsymmetrical Dinuclear Mixed-Valence Complex for surface binding. *Inorg. Chem.* 42 (2003), 5707–5714.
- M. Ottavi, M. Momenzadeh, and F. Lombardi. 2005. Modeling QCA Defects at Molecular-level in Combinational Circuits. In *20th IEEE international Symposium on Defect and Fault Tolerance in VLSI system (DFT)*. IEEE, New York, USA.
- P. Motto, M. Crepaldi, G. Piccinini, and D. Demarchi. 2014. NanoCube: A low-cost, modular, and high-performance embedded system for adaptive fabrication and characterization of nanogaps. *IEEE Transactions on Nanotechnology* 13, 2 (2014), 322–334.
- A. Pulimeno. 2013. PhD dissertation, Polytechnic of Turin. (2013).

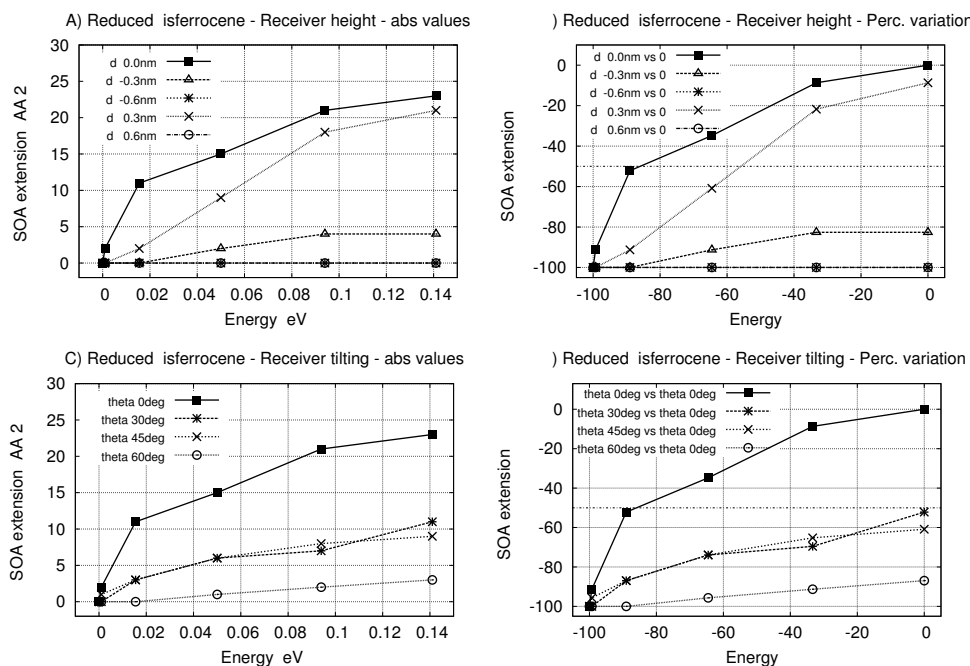


Fig. 16. SOA as a function of energy, for Oxidized molecule calculated in absolute (A,B) and percentage (C,D) value. Results obtained for different receiver height (A,C) and for different receiver tilt angle (B,D) are compared.

- A. Pulimeno, M. Graziano, C. Abrardi, D. Demarchi, and G. Piccinini. 2011. A write-in system based on electric fields for Molecular QCA. In *2011 IEEE International NanoElectronics Conference (INEC)*. IEEE, Tao-Yuan, Taiwan, 1–2.
- A. Pulimeno, M. Graziano, A. Antidormi, R. Wang, A. Zahir, and G. Piccinini. 2014. Understanding a Bis-ferrocene Molecular QCA Wire, In *Field-Coupled Nanocomputing. LECTURE NOTES IN COMPUTER SCIENCE* (2014), 307–338.
- A. Pulimeno, M. Graziano, D. Demarchi, and G. Piccinini. 2012. Towards a molecular QCA wire: simulation of write-in and read-out systems. *Solid State Electronics* 77 (2012), 101–107.
- A. Pulimeno, M. Graziano, and G. Piccinini. 2012. UDSM Trends Comparison: From Technology Roadmap to UltraSparc Niagara2. *IEEE Transactions on VLSI systems* 20, 7 (July 2012).
- A. Pulimeno, M. Graziano, A. Sanginario, V. Cauda, D. Demarchi, and G. Piccinini. 2013a. Bis-ferrocene molecular QCA wire: ab-initio simulations of fabrication driven fault tolerance. *IEEE Transactions on Nanotechnology* 12, 4 (2013).
- A. Pulimeno, M. Graziano, R. Wang, D. Demarchi, and G. Piccinini. 2013b. Charge Distribution in a Molecular QCA Wire based on Bisferrocene Molecule. In *Nanoarch 2013*. IEEE. <http://porto.polito.it/2511682/>
- H. Qi, S. Sharma, Z. Li, G. L. Snider, A. O. Orlov, C.S. Lent, and T.P. Fehlner. 2003. Molecular Quantum Cellular Automata Cells, Electric Field Driven Switching of a Silicon Surface Bound Array of Vertically Oriented Two-Dot Molecular Quantum Cellular Automata. *Journal of American Chemical Society* 125 (2003), 15250–15259.
- I. Rattalino, P. Motto, G. Piccinini, and D. Demarchi. 2012. A new validation method for modeling nanogap fabrication by electromigration, based on the Resistance-Voltage (R-V) curve analysis. *Physics Letters, Section A: General, Atomic and Solid State Physics* 376, 30-31 (2012), 2134–2140.
- G. Schulhof, K. Walus, and G.A. Jullien. 2007. Simulation of Random Cell Displacement in QCA. *ACM journal on emerging Technologies in Computing system* 3, 1 (2007).
- U.C. Singh and P.A. Kollman. 1984. An approach to computing electrostatic charges for molecules. *Journal on Computational Chemistry* 5 (1984), 129–145.

- S. Strobel, S. Harrer, G. Penso Blanco, G. Sacrpa, G. Abstreiter, P. Luigi, and M. Tornow. 2009. Planar Nanogap Electrodes by Direct Nanotransfer Printing. *Small* 5 (2009).
- M.B. Tahoori, M. Momenzadeh J. Huang, and F. Lombardi. 2004. Testing of Quantum Cellular Automata. *IEEE Transaction on nanotechnology* 3, 4 (2004).
- M. Vacca, M. Graziano, and M. Zamboni. 2011. Asynchronous Solutions for Nano-Magnetic Logic Circuits. *ACM J. on Emerging Tech. in Comp. Systems* 7, 4 (December 2011).
- M. Vacca, M. Graziano, and M. Zamboni. 2012. Majority Voter Full Characterization for Nanomagnet Logic Circuits. *IEEE T. on Nanotechnology* 11, 5 (Sept. 2012), 940–947. DOI:<http://dx.doi.org/10.1109/TNANO.2012.2207965>
- M. Vacca, J. Wang, M. Graziano, M.R. Roch, and M. Zamboni. 2014. Feedbacks in QCA: A Quantitative Approach. *Very Large Scale Integration (VLSI) Systems, IEEE Transactions on PP*, 99 (2014), 1–1.
- K. Walus. QCA Designer Reference Manual <http://www.mina.ubc.ca/qcadesigner-manual>. (????).
- X. Yang, L. Cai, S. Wang, Z. Wang, and C. Feng. 2012. Reliability and Performance Evaluation of QCA Devices With Rotation Cell Defect. *IEEE Transaction on nanotechnology* 11, 5 (2012).
- A. Zahir, S. A. A. Zaidi, A. Pulimeno, M. Graziano, D. Demarchi, G. Masera, and G. Piccinini. 2014. Molecular transistor circuits: From device model to circuit simulation. In *Nanoscale Architectures (NANOARCH), 2014 IEEE/ACM International Symposium on*. IEEE, 129–134.